JOURNAL OF AIRCRAFT
Vol. 39, No. 6, November–December 2002

Effects of Reynolds Number on Flow over 76/40-Degree Double-Delta Wings

Niek G. Verhaagen*
Delft University of Technology, 2600 GB Delft, The Netherlands

The effects of the Reynolds number on the flow over 76/40-deg double-delta or strake-wing configurations and the capability of numerical solutions to predict these effects are discussed. The flow over the strake appears to be little affected by the Reynolds number. On the wing strong effects are evident on the flow on and off the wing surface. Numerical solutions tend to reasonably well predict the flow over these types of configurations.

Nomenclature

b	=	wing span
C_p	=	static-pressure coefficient
c	=	root chord length
M	=	freestream Mach number
Re	=	Reynolds number, per meter chord
Re_c	=	Reynolds number, based on root chord
s	=	local wing semispan
x, y, z	=	coordinates of wing-axes system, origin at apex
α	=	geometric angle of attack
α_e	=	effective angle of attack

Introduction

DOUBLE-DELTA or strake-wing configurations are employed for several modern fighter aircraft to obtain a high maneuverability. The highly swept strake is an additional lifting surface above which a stable vortex is formed. This vortex stabilizes the flow over the wing and enhances the lift-to-drag efficiency of the aircraft. The shedding, interaction, and breakdown of the vortices formed over the strake and wing depend on the aircraft geometry and flight conditions. Apart from the beneficial effect of enhancing the aircraft lift and maneuverability, these vortices may also contribute to serious structural fatigue problems, such as the tail-buffet problem of fighter aircraft.

The basic planform representative of highly maneuverable strake-wing aircraft is characterized by a strake and wing leading-edge sweep angle of 76 and 40 deg, respectively, and a strake-wing leading-edge junction at approximately midchord.[1]

Numerical solutions of the flow over this type of planform were obtained by, among others, Kern,[1] Hsu and Liu,[2] and Ekaterinaris et al.[3] Some of their predictions are given in Fig. 1. The solutions show shedding of the vortices from the strake and wing leading edges and a strong interaction and breakdown of these vortices over the wing panel. To validate the numerical predictions obtained by Kern,[1] extensive experimental studies were conducted on a 76/40-deg double-delta-wing model constructed by the Naval Air Warfare Center (NAWC). This model was tested at different test conditions in wind tunnels at NAWC and NASA Langley Research Center (LaRC). Results of the tests conducted in the Basic Aerodynamics Research Tunnel (BART) at NASA LaRC have been published by Verhaagen et al.[4] The tests showed that the flow over the double-delta wing is sensitive to Reynolds-number effects. Evidence of these effects is also obtained from experimental studies conducted by Hebbar et al.[5] and Rogers and Verhaagen[6] on similarly shaped double-delta-wing models.

An overview of the effects of the Reynolds number on the flow over straight leading-edge delta wings is given by Visser and Washburn.[7] Although the majority of the vortex flow over these wings is dominated by potential flow effects, viscous effects remain limited to a small subcore region and the upper-surface boundary layer. The core axial velocities were observed to be dependent, the onset of breakdown to be independent of the Reynolds number. Effects were further evident on the upper-surface flow and pressure distribution caused by the transition of the boundary layer on this surface.

The objective of the present paper was to discuss the effects of the Reynolds number on the flow over 76/40-deg double-delta wings and the capability of numerical solutions to predict these effects. In the paper first the effects of the Reynolds number on the flow over this type of double-delta wings are described using data obtained on the NAWC model and on other models of identical geometry. Subsequently, available numerical solutions for the flow about these configurations are discussed.

Test Data Results

Off-Surface Flow

The geometry of the 76/40-deg swept NAWC model is shown in Fig. 2. The leading-edge kink was situated at 52% chord. The wing tip was cropped from the 84% chordwise station. The sharp leading and trailing edges of the model were broken and rounded to a diameter of 0.13 mm (0.005 in.). The under surface was beveled at 20 deg over a width of 26.16 mm. Pressure taps were drilled on the left side of the model at 25, 75, and 90% chord. The model was tested in the BART; this is a subsonic, open-return wind tunnel with a test section 0.71 m high, 1.02 m wide, and 3.05 m long (Ref. 8). In this paper, only test data that help illustrate the effects of the Reynolds number are shown. More test details and results can be found in the original data reports.[4]

A smoke/laserlight-sheet technique was used to illuminate the trajectories and breakdown locations of the strake- and wing-vortex cores. Figure 3 shows the vortices at a geometric $\alpha = 10$ deg. The light sheet is in the plane of the vortices. The visualization tests were conducted at $Re = 1.23 \times 10^6$/m ($Re_c = 0.5 \times 10^6$). The effect of the angle of attack on the vortex core trajectory and breakdown point is shown in Fig. 4. The interaction between the strake and wing vortices can be seen to increase with α. The vortices were observed to burst before they cross over. The wing-vortex cores burst earlier than the strake-vortex cores. Similar tendencies have been observed in experiments carried out on an identically shaped double-delta wing model by Hebbar et al.[5] Their model had a chord length of 237 mm and was tested in a water tunnel at $Re = 6.33 \times 10^4$, 1.9×10^5, and 3.16×10^5/m at α from 5 to 30 deg. In these experiments a

Presented as Paper 99-3117 at the AIAA 17th Applied Aerodynamics Conference, Norfolk, VA, 28 June–1 July 1999; received 31 July 2000; revision received 7 February 2002; accepted for publication 18 March 2002.

*Research Scientist, Department of Aerospace Engineering, P.O. Box 5058; n.g.verhaagen@lr.tudelft.nl. Senior Member AIAA.

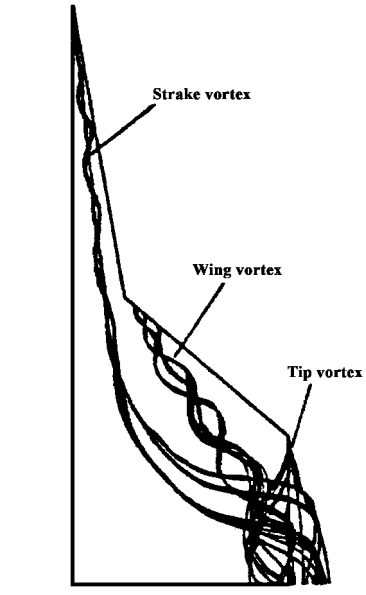

a)

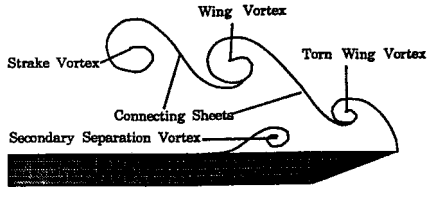

b)

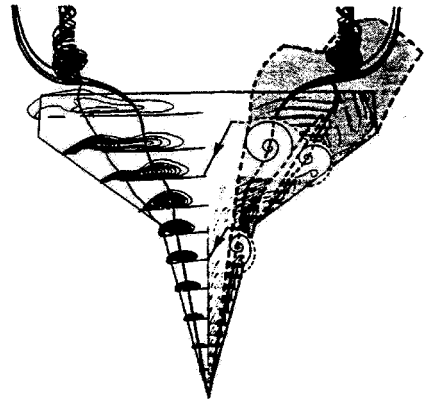

c)

Fig. 1 Solutions for the flow over double-delta wings: a) solution by Hsu and Liu [2]; $M = 0.1$, $\alpha = 20$ deg, and $Re_c = 1.3 \times 10^6$, b) solution by Kern [1]; $M = 0.2$, $\alpha = 22.5$ deg, and $Re_c = 1 \times 10^6$, and c) solution by Ekaterinaris, et al [3]; $M = 0.22$, $\alpha = 19$ deg, and $Re = 4 \times 10^6$.

strong interaction between the strake and wing vortices was observed at $Re = 6.33 \times 10^4$ (Fig. 5). At this Reynolds number a rapid inboard displacement of the wing vortex is evident downstream of the leading-edge kink at all angles of attack considered. Laser Doppler velocimetry measurements indicate that this is a result of the occurrence of a large separated flow region on the outer wing panel. At the two larger Reynolds numbers there is only a weak interaction between the strake and wing vortices. These vortices were observed to move outboards and closer to the wing surface with increasing Reynolds number.

The topology of the crossflow around the strake and wing panels is given in Fig. 6. The flow around the strake is similar to that around a straight leading-edge delta wing. The flow over the wing panel is characterized by the presence of distinct strake and wing primary and secondary vortices. The occurrence of the strake secondary vortices over the wing panel depends on the angle of attack and Reynolds number. The effect of the angle of attack on the crossflow over the

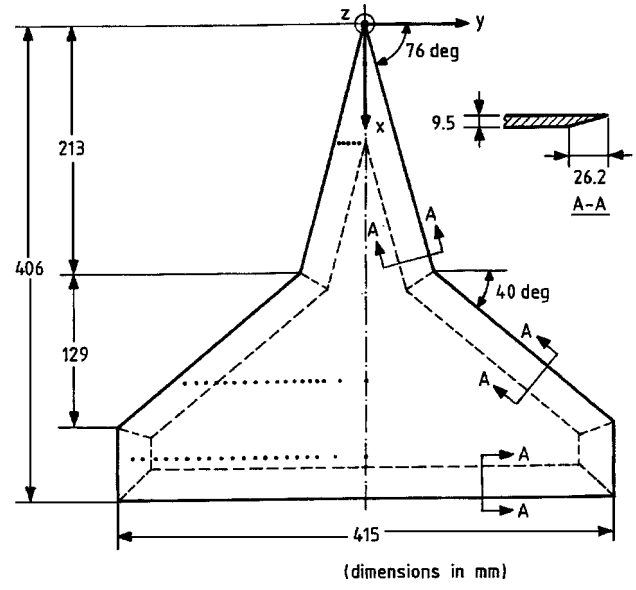

Fig. 2 NAWC double-delta wing geometry.

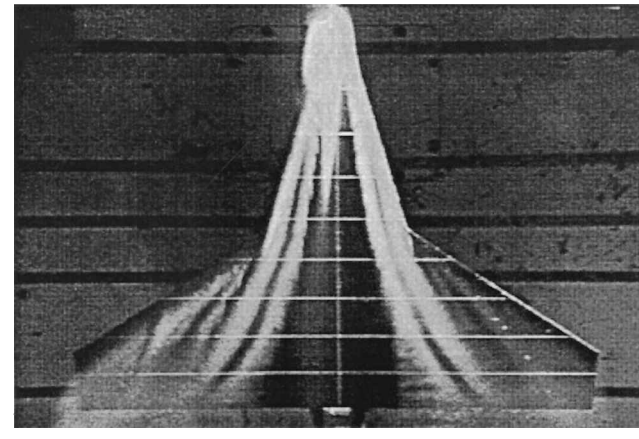

Fig. 3 Vortices illuminated by laserlight sheet at $\alpha = 10$ deg.

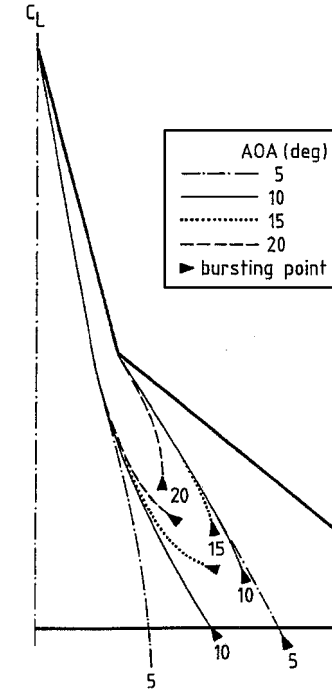

Fig. 4 Effect of α on vortex-core trajectory and breakdown point; $Re = 1.23 \times 10^6$/m.

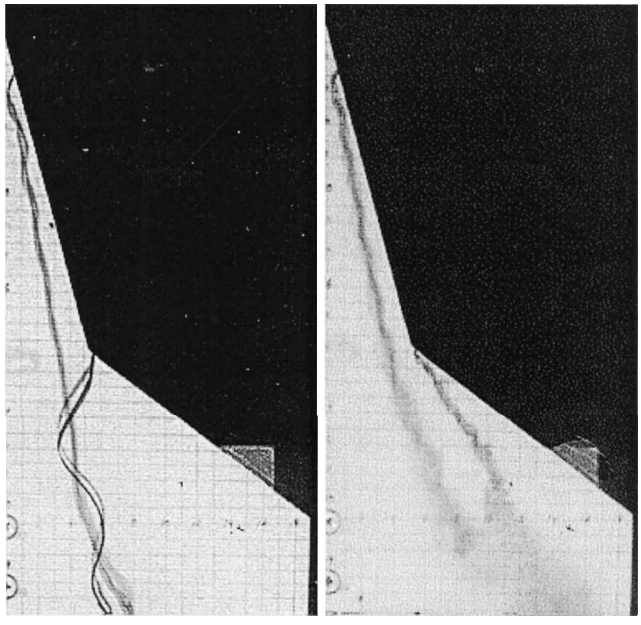

Fig. 5 Effect of Reynolds number on the interaction of vortices over a 76/40-deg double-delta wing at α = 10 deg (Ref. 5); $Re = 6.33 \times 10^4$/m (left-hand picture) and 3.16×10^5/m (right-hand picture).

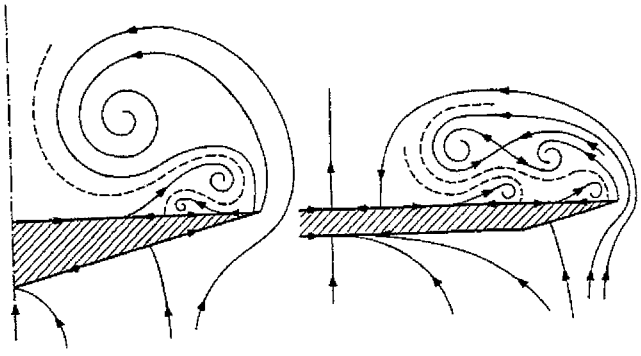

Fig. 6 Topology of crossflow over strake (left-hand sketch) and wing panel (right-hand sketch).

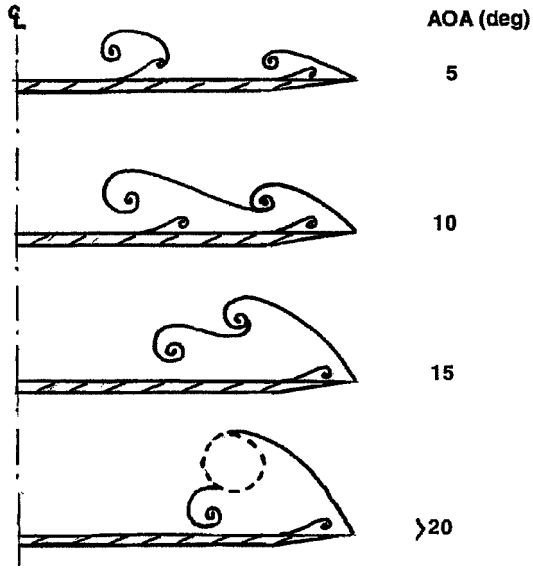

Fig. 7 Effect of α on crossflow topology at 75% chord; $Re < 3.0 \times 10^6$/m.

NAWC model was studied up to $\alpha = 25$ deg. No effect was observed on the topology of the crossflow over the strake. Figure 7 shows the effect on the crossflow over the wing panel at 75% chord. Separate strake and wing primary and secondary vortices were observed to exist up to at least $\alpha = 10$ deg. Beyond this angle, the strake and wing vortices start to coil around each other, whereas at $\alpha = 20$ deg breakdown of the wing-vortex core occurs. Secondary separation takes place only near the leading edge.

In the BART the effect of the Reynolds number was studied on only the breakdown point of the strake-vortex core at $\alpha = 20$ deg. The Reynolds number was varied between 0.62 and 4.93×10^6/m, but no effect on the breakdown point of the strake-vortex core was observed in this range. In the experiments conducted by Hebbar et al.[5] at lower Reynolds numbers, however, a displacement of the strake- and wing-vortex breakdown location toward the apex of the model is evident as Reynolds number is increased.

Surface Flow

Visser and Washburn[7] studied the effect of the Reynolds number on the surface-flow pattern of a 76-deg delta wing at $\alpha = 20$ deg. Their model had a chord length of 457 mm. Figure 8 shows the effect of Re_c on the transition of the boundary layer on the upper surface. An increase of the Reynolds number tends to decrease the distance from the boundary-layer transition region to the apex. The latter region is characterized by a kink in the secondary-separation line caused by the, in comparison to the laminar separation, retarded separation of the turbulent boundary layer.

Figure 9 shows the boundary-layer flow pattern on the NAWC wing at $Re = 2.46 \times 10^6$/m for $\alpha = 10$ and 22.5 deg. The pattern was visualized using an oil-flow mixture consisting of titanium dioxide and kerosene. On the strake there is not much difference between the patterns at these two angles. The boundary layer underneath the strake vortex separates at a spanwise position $y/s \approx 0.70$, indicating that the boundary layer is laminar. In the case of a turbulent boundary layer, separation would occur more outboard at $y/s \approx 0.85$ (Fig. 8). A tertiary-separation line was visible from near the apex to the leading-edge kink.

The shear-flow patterns induced by the strake and wing vortices and accompanying secondary-separation lines on the wing panel remain individually distinguishable up to the trailing edge. Beyond $\alpha = 10$ deg the strake-vortex secondary-separation lines vanish starting at the trailing edge, indicating that the secondary separation is suppressed (Fig. 7). Both the strake- and wing-vortex cores break down over the wing (Fig. 4). As can be noted from the pattern at $\alpha = 22.5$ deg, just upstream of the breakdown point of the strake vortex the oil-flow pattern gives evidence of the strong outward bending of this vortex induced by the wing vortex. Downstream of the breakdown point a wide region of turbulent shear flow is visible. Outboard of the wing-vortex secondary-separation line elongated regions of accumulated and circulating surface fluid were observed.

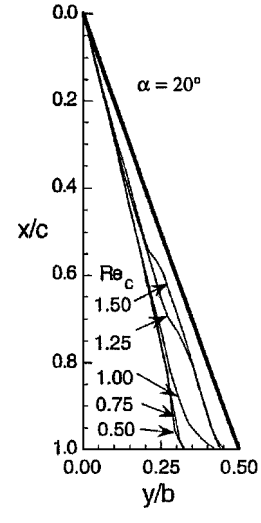

Fig. 8 Effect of Re_c on the transition of the boundary layer on a 76-deg delta wing at α = 20 deg (Visser and Washburn[7]).

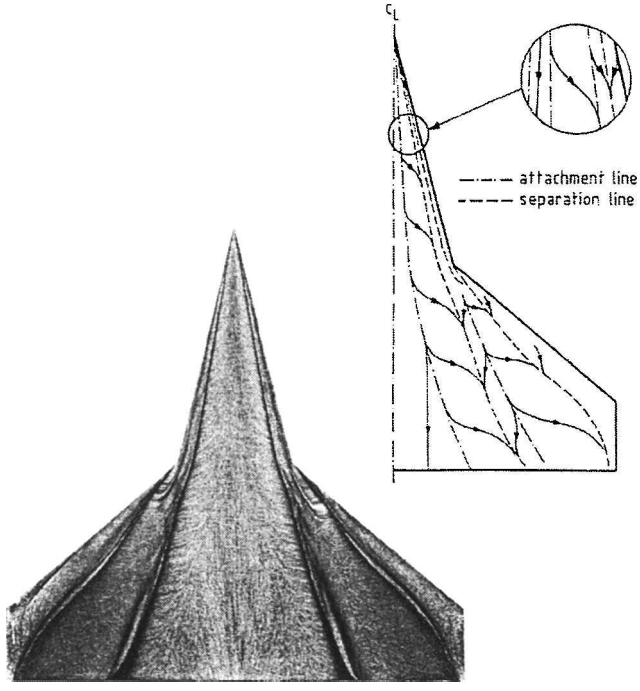

α = 10 deg

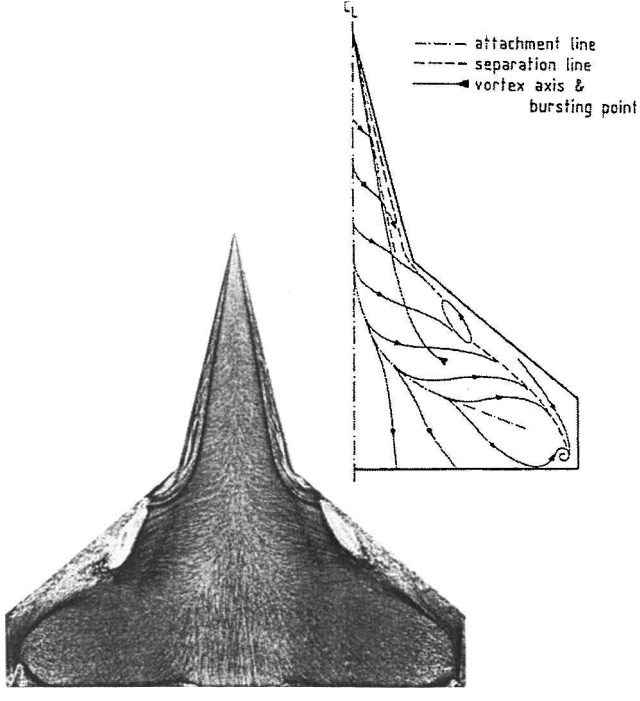

α = 22.5 deg

Fig. 9 Upper-surface shear-flow pattern at various α; $Re = 2.46 \times 10^6$/m.

These regions tend to move toward the kink with increasing angle of attack. Near the tip a focus was observed in the shear-flow pattern. This focus induced an upstream flow locally at the trailing edge.

As far as the effect of the Reynolds number is concerned, on the strake the shear-flow pattern changes little as the Reynolds number increases from 1.23 to 3.69×10^6/m. This holds for α up to 25 deg. There was no sign of transition of the boundary-layer underneath the strake vortex from laminar to turbulent flow. As can be seen from Fig. 10, on the wing panel the strake-vortex secondary-separation lines are clearly visible at $\alpha = 10$ deg, if $Re = 1.23$ and 2.46×10^6/m. From about the 65% chordwise position the secondary-separation lines at the latter Reynolds number are located outboard those at the lower Reynolds number. This is supposed to be caused by the transition of the boundary layer underneath the strake vortex. The secondary-separation lines have vanished at $Re = 3.69 \times 10^6$/m, indicating that no secondary vortices are induced by the strake vortices at this Reynolds number. At $\alpha = 22.5$ deg a Reynolds-number effect was visible on only the location of the wing-vortex secondary-separation lines. These lines tend to bend outboard with increasing Reynolds number as a result of the transition of the boundary layer underneath the wing vortex.

Surface-Pressure Distribution

The effect of the Reynolds number on the static-pressure distribution of a wing is related to the nature of the boundary layer over the wing. Hummel[9] was one of the first to study this for the case of a 76-deg delta wing. As illustrated in Fig. 11, at low Reynolds number a laminar boundary layer exists on the upper surface that separates into a large secondary vortex. The latter vortex induces a suction peak almost as strong as that of the primary vortex. At high Reynolds number the boundary layer on the upper surface is turbulent, and the more outboard separation results into a smaller secondary vortex and suction peak. Associated with this is a primary vortex that is located more outboard and closer to the wing surface. As a result, the suction induced by the latter vortex is larger than in the laminar case. The shape of the C_p curve hence is indicative for the nature of the boundary-layer flow on the upper surface of a delta wing. Visser and Washburn[7] confirm the effect of the boundary layer on the position of the vortices over a 76-deg delta wing. They further found that the flowfield of the primary vortex remained relatively unchanged. The vorticity levels and distributions were equivalent for both boundary-layer states, indicating that the primary-vortex flowfield is insensitive to the Reynolds number.

The upper plot of Fig. 12 shows the effect of angle of attack on the C_p curves at the upper surface of the NAWC model at 25% chord for $Re = 2.46 \times 10^6$/m. The size and circulation of the strake vortex increase with the angle of attack, resulting in a growing suction peak. The level of suction induced by the secondary and tertiary vortices is about the same as that induced by the primary vortex, confirming that the boundary layer underneath this vortex remains laminar up to at least $\alpha = 25$ deg, which was the largest α tested in the BART experiment.

The effect of the angle of attack on the C_p curves at 75% chord is shown in the lower plot of Fig. 12. The changes with α correspond with those of the crossflow (Fig. 7). The shape of the C_p curves indicates that the boundary layer underneath the strake vortex remains laminar up to at least $\alpha = 10$ deg, whereas the boundary layer underneath the wing vortex remains laminar up to at least $\alpha = 5$ deg if $Re = 2.46 \times 10^6$/m.

The effect of the Reynolds number on the C_p curves was investigated at $\alpha = 10$ deg. This α was chosen because numerical solutions were obtained for this angle. Pressures were recorded at Reynolds numbers ranging from 1.23 to 3.69×10^6/m. The effect on the C_p distribution at 25% chord was found to be very small, of the order of the measurement accuracy. Figure 13 shows the distributions at 75% chord for $Re = 1.23 \times 10^6$/m (solid curve) and 3.69×10^6/m (dashed curve). A clear effect is evident in the region dominated by the strake vortex. Because of the transition of the boundary layer underneath this vortex, the secondary vortex and its suction have vanished at $Re = 3.69 \times 10^6$/m. This is in accordance with the surface oil-flow pattern, which showed no strake secondary-separation markings at this Reynolds number. As a result of this, the strake vortex is presumed to be located closer to the wing surface and to induce a higher suction than at $Re = 1.23 \times 10^6$/m. Underneath the wing vortex, transition of the boundary layer results in a smaller and more outboard located secondary vortex. As a consequence, the primary wing vortex can be expected to move slightly outboard as well, explaining the slight outboard shift of the wing-vortex suction peak as the Reynolds number increases from 1.23 to 3.69×10^6/m. Similar to the strake vortex, the wing vortex is presumed to move closer to the wing and to induce a higher suction peak, compared to the situation at $Re = 1.23 \times 10^6$/m. Because on the NAWC model there were (too) few orifices on the surface underneath the wing vortex, the latter tendency could not be confirmed from the C_p data. Clear

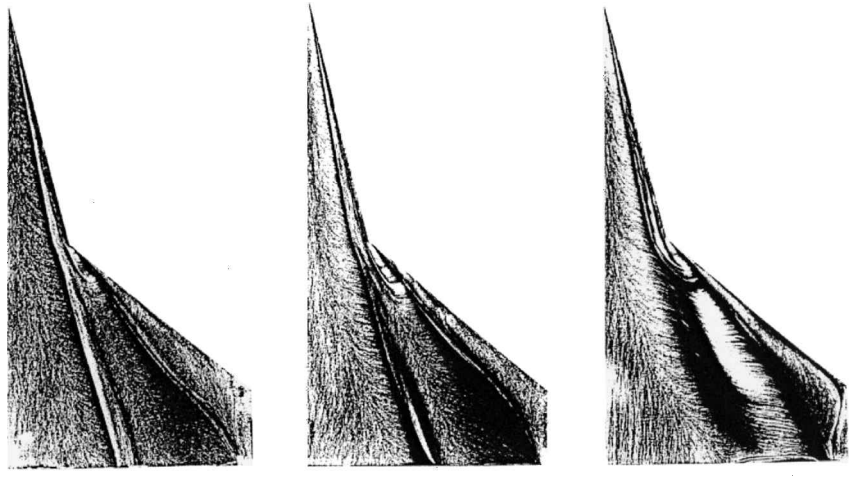

$Re = 1.23, 2.46$ and 3.69×10^6/m

Fig. 10 Effect of Reynolds number on upper-surface oil-flow pattern at α = 10 deg.

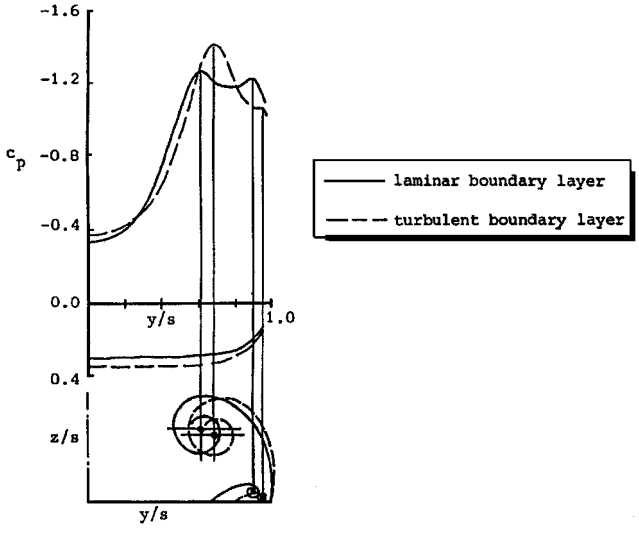

Fig. 11 Effect of boundary-layer transition on the vortex flow and pressure distribution of a 76-deg delta wing (Ref. 9).

evidence of this tendency, however, is obtained from data recorded by Rogers and Verhaagen[6] on a 76/40-deg double-delta wing with a larger number of pressure taps on the wing panel.

Numerical Solutions

Solutions for the flow around the NAWC double-delta wing in free air were obtained by Kern using the compressible thin-layer Navier–Stokes solver OVERFLOW. The flow was solved on a spherical C-O type field grid with an embedded grid on the leeward side of the double-delta wing. The dimensions of the embedded grid were $255 \times 177 \times 73$, and the composite grid totaled about 3.4 million points. The solutions were obtained at an effective angle of attack $\alpha_e = 10$ deg, $M = 0.2$, and $Re = 1.23 \times 10^6$/m with completely laminar flow. Further details of the computations are given in the data reports.[4]

The predicted upper-surface streamline pattern is compared with the oil-flow pattern in Fig. 14. The oil-flow pattern was obtained at also $Re = 1.23 \times 10^6$/m and at a geometric $\alpha = 8$ deg. If tunnel-wall and model-support interference effects are taken into account, α_e is estimated to be as large as 11 deg (Ref. 10). On the strake the secondary-separation and tertiary-separation lines are well predicted. At the kink the shear flow resembles the experiment, in that the strake-vortex tertiary-separation line vanishes, while the flow is entrained outboard toward the wing-vortex secondary-separation

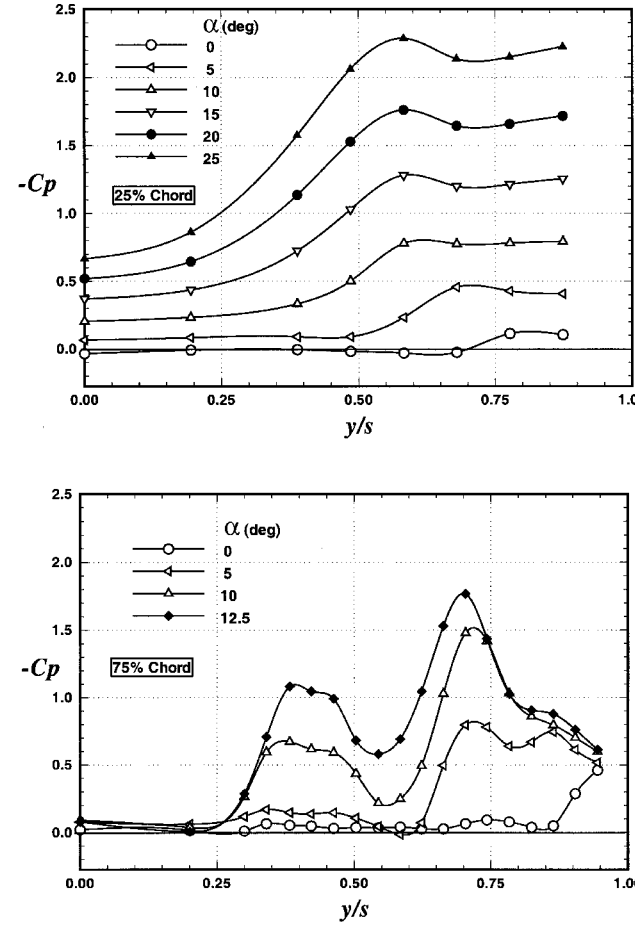

Fig. 12 Effect of α on upper-surface C_p at 25 and 75% chord; $Re = 2.46 \times 10^6$/m.

line. A slight outboard bending of the strake-vortex secondary-separation line near the kink, caused by the influence of the formation of the wing vortex, is also predicted. Over the wing panel the location of the predicted strake-vortex secondary-separation line correlates well with that of the experiment. The boundary-layer flow underneath the strake vortex is laminar in the experiment. Downstream of the 85% chordwise location, the predicted secondary-separation line bends inboard to become parallel to the centerline at the trailing edge. The wing-vortex secondary-separation line is predicted inboard of the experimental position. The outboard bending

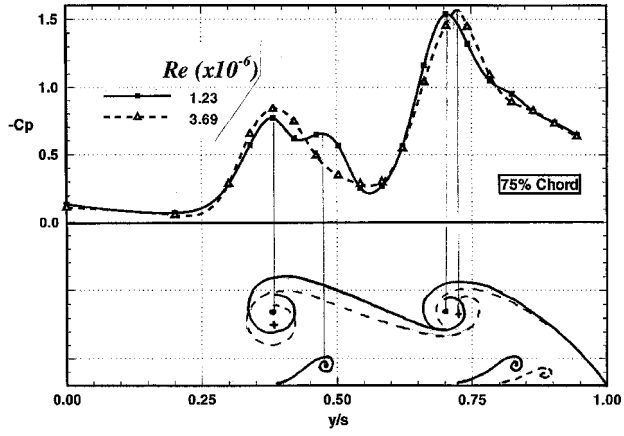

Fig. 13 Effect of Reynolds number on upper-surface C_p and crossflow structure at 75% chord; α = 10 deg.

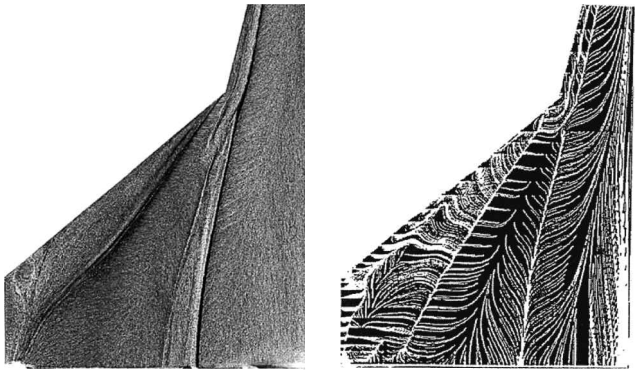

Experiment; α_e = 11 deg **Solution; α_e = 10 deg**

Fig. 14 Comparison of visualized and predicted upper-surface shear-flow pattern for $Re = 1.23 \times 10^6$/m.

of this separation line noted in the experiment was caused by the transition from laminar to turbulent flow. Because the flow simulated was purely laminar, this outboard bending could not be predicted. For the surface shear-flow pattern a turbulent-flow solution was not available at the time this paper was written. Fully laminar and fully turbulent solutions, however, were generated for the surface-pressure distributions.

Figure 15 compares the measured and predicted C_p data at 25 and 75% chord for $\alpha_e = 10$ deg. The experimental data were acquired at $Re = 2.46 \times 10^6$/m and were corrected for tunnel-wall and model-support interference effects.[10]

At 25% chord (upper plot) the flow is laminar in the experiment. The test data (circles) are therefore compared to the laminar-flow solution (solid curve). This solution can be seen to predict the location of the primary vortex well and to predict a higher level of C_p in the region dominated by vortices.

At 75% chord the shape of the C_p curve through the test data gives evidence of a laminar boundary layer underneath the strake vortex and a turbulent layer underneath the wing vortex. The data at this station are therefore compared with the solutions for the case of fully laminar and of fully turbulent flow (solid and dashed curve, respectively). Compared to the laminar-flow case, the turbulent-flow solution was obtained at a twice as high Reynolds number. The turbulent flow was simulated using the Baldwin–Barth one-equation turbulence model. As far as the strake vortex is concerned, compared to the experiment both solutions predict a more outboard position, a higher suction induced by the primary vortex and a lower suction induced by the secondary vortex. Larger differences can be noted in the region dominated by the wing vortex. Compared to the laminar-flow case, the turbulent-flow solution predicts a slightly more outboard location and a higher suction for the latter vortex. In the experiment a lower suction was recorded. Outboard of the wing

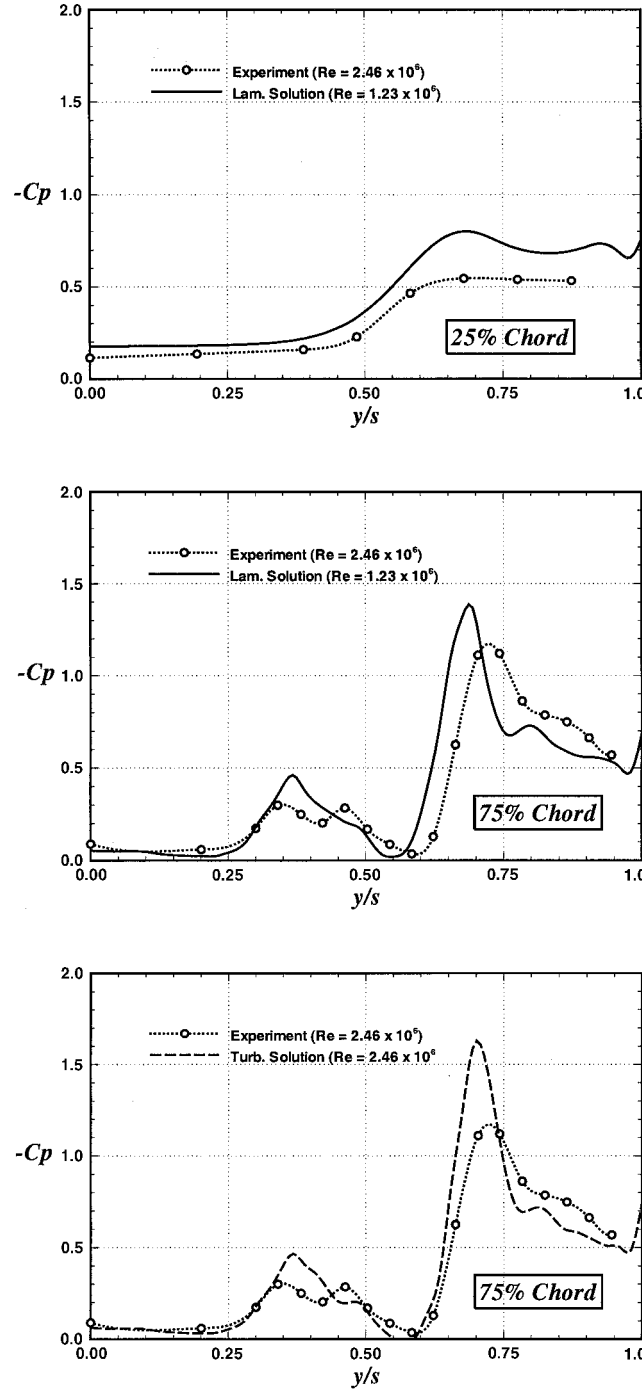

Fig. 15 Comparison of measured and predicted upper surface C_p at 25 and 75% chord; α_e = 10 deg.

primary vortex the solution was unreliable because of a lack of convergence. Time-accurate solutions would be required to capture the time evolution of the flow in this region.

Ekaterinaris et al.[3] solved the flow over a 76/40-deg double-delta wing that was tested at the Dutch National Aerospace Laboratory (NLR) by Cunningham and Den Boer.[11] The thickness distribution of their double-delta wing was different from that of the flat NAWC model. The NLR model had a strake with a diamond cross section, while the wing was formed by NACA 64A005 sections. The chord length was 784 mm. The flow was solved on a spherical C-O type field grid using compressible thin-layer Navier–Stokes equations. Solutions were obtained at $\alpha = 10$, 19 and 22.4 deg, $M = 0.22$, and $Re = 5.1 \times 10^6$/m ($Re_c = 4.0 \times 10^6$). These conditions match those of the experiment. Because boundary-layer transition was expected to occur very close to the apex at this high Reynolds number, solutions were obtained with only fully turbulent flow. This

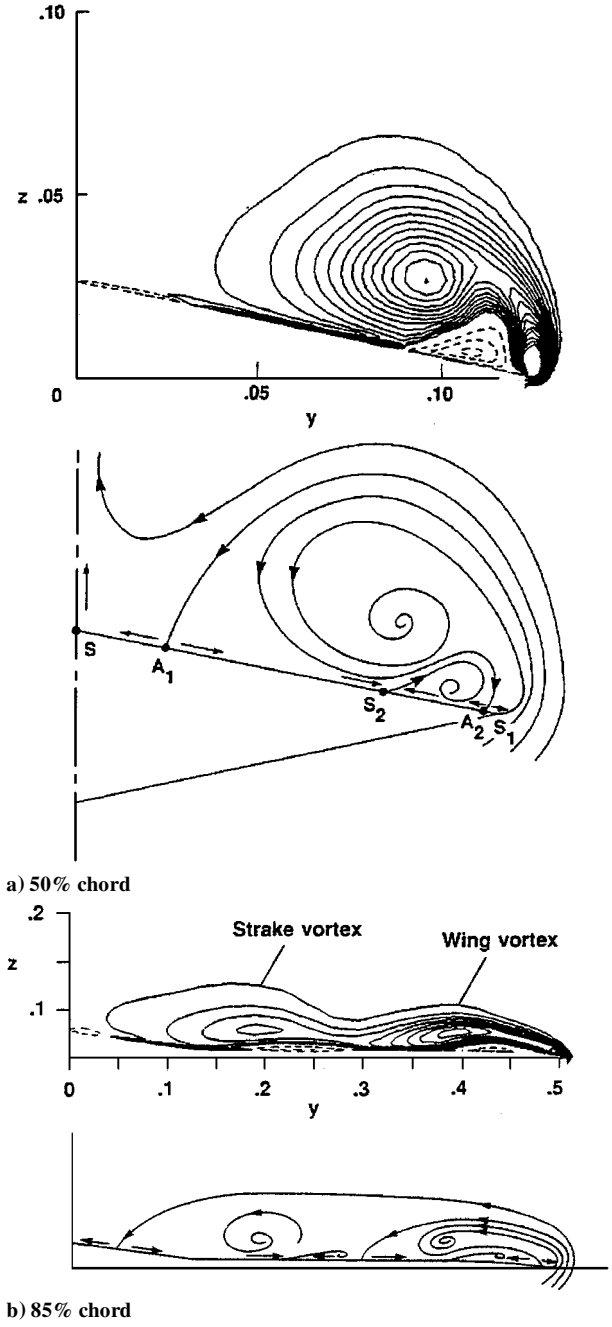

a) 50% chord

b) 85% chord

Fig. 16 Helicity contours and crossflow pattern at various chordwise stations, α = 10 deg and $Re_c = 4.0 \times 10^6$ (Ref. 3).

was simulated using the Baldwin–Lomax eddy-viscosity model, as modified by Degani and Schiff. The solutions were performed in a time-accurate manner, and convergence of three orders of magnitude of the residuals was achieved.

The solutions for the flow at $\alpha = 10$ deg were computed on a $82 \times 63 \times 64$ point grid. The solutions for the helicity contours (upper plot) and crossflow pattern (lower plot) at 50 and 85% chord are depicted in Fig. 16. As shown in Fig. 16a, at 50% chord primary and secondary vortices were predicted. Contrary to Kern's solution for the flow over the strake of the NAWC model, a tertiary vortex was not solved. This may be because the boundary layer on the strake was taken turbulent in the computations or a too coarse grid. Figure 17a compares the predicted and measured C_p for 40% chord. Note that Ref. 6 in the plot is identical to Ref. 11 used here. The level and location of the suction induced by the primary vortices are reasonably well predicted. The shape of the predicted and measured C_p curve is not typically that of a turbulent boundary-layer flow, characterized by a weak secondary separation (Fig. 11). Figure 16b shows the predicted flow over the wing panel at 85% chord. A distinct strake and wing primary- and secondary-vortex system is predicted, which appears to correspond with the distinct suction peaks in the measured C_p curve (Fig. 17b). On the flat NAWC model the strake secondary vortex was observed to vanish beyond $Re = 2.46 \times 10^6$/m.

The solution at $\alpha = 19$ deg was obtained on the $82 \times 63 \times 64$ point grid and on a $82 \times 117 \times 64$ point grid to provide increased

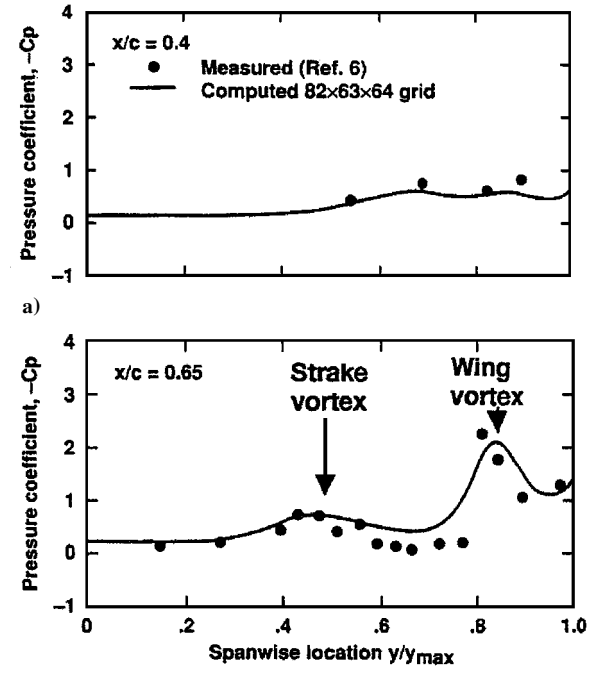

Fig. 17 Comparison of predicted and measured upper-surface C_p at a) 40% and b) 65% chord for α = 10 deg and $Re_c = 4.0 \times 10^6$ (Ref. 3).

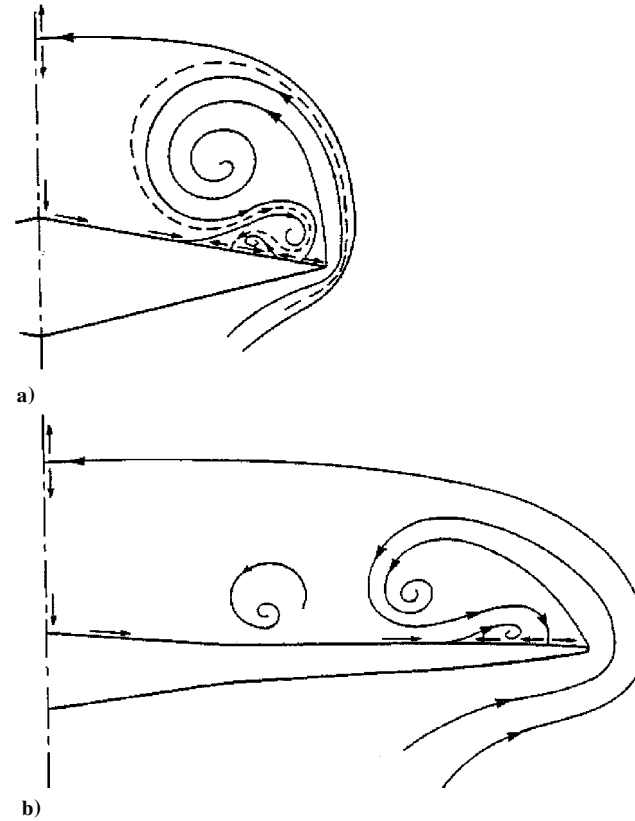

Fig. 18 Crossflow pattern on a) the strake and b) the wing for α = 19 deg and $Re_c = 4.0 \times 10^6$ (Ref. 3).

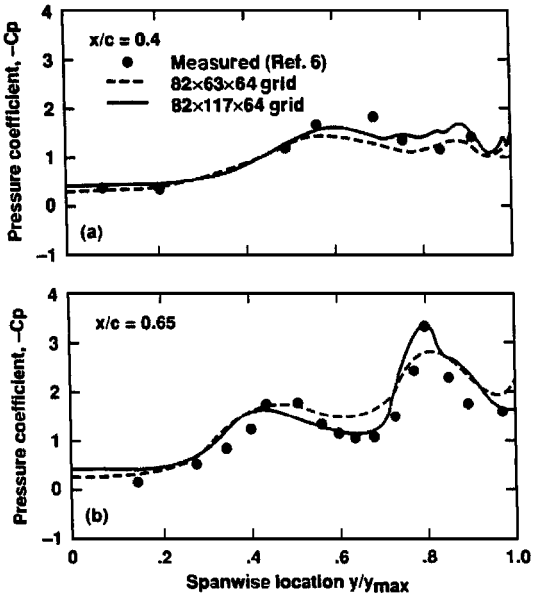

Fig. 19 Comparison of predicted and measured upper-surface C_p at a) 40% and b) 65% chord for $\alpha = 19$ deg and $Re_c = 4.0 \times 10^6$ (Ref. 3).

resolution in the circumferential direction. Figure 18 shows the crossflow pattern predicted over the strake and wing panel. Figure 19 compares the predicted and measured upper surface C_p at 40 and 65% chord. The fine-grid solutions (solid curves) predict the location of the strake and wing vortices reasonably well. Differences are apparant in the level of the predicted and measured suction peaks. A perspective view of the flow on and off the upper surface was given in Fig. 1c.

Conclusions

Based on existing experimental data sets generated at angles of attack up to 25 deg and at Reynolds numbers up to 4×10^6, it can be concluded that the flow over the strake panel of a 76/40-deg double-delta wing is little affected by the Reynolds number. The boundary-layer flow on the upper surface of this panel remains laminar.

On the wing panel, at Reynolds numbers below 10^5/m strong Reynolds-number effects were observed on the interaction between the strake and wing vortices. At larger Reynolds numbers, the interaction between these vortices is weak at low α and strong if α is larger than 10 deg. Few data are available on the effect of the Reynolds number on the breakdown point of the strake- and wing-vortex cores. At Reynolds numbers below 3.2×10^5/m, this point was observed to move toward the apex with increasing Reynolds number, whereas at higher Reynolds number no effect was observed. Viscous effects dominate the boundary layer and, associated with this, the pressure distribution on the upper surface of the wing panel.

Numerical solutions for 76/40-deg double-delta wings are available for a limited number of Reynolds number, α combinations. The predicted flow on and off these wings shows a reasonably good agreement with the experiment. Differences are evident in the level of the predicted and measured upper-surface pressures and are likely caused by insufficient grid resolution and turbulence modeling.

The existing solutions were obtained some years ago. It would be interesting to have solutions available generated by state-of-the-art flow models.

References

[1]Kern, S. B., "Numerical Investigation of Vortex Flow Control Through Small Geometry Modifications at the Strake/Wing Junction of a Cropped Double-Delta Wing," AIAA Paper 92-0411, Jan. 1992

[2]Hsu, C.-H., and Liu, C. H., "Upwind Navier–Stokes Solutions for Leading-Edge Vortex Flows," AIAA Paper 89-0265, Jan. 1989.

[3]Ekaterinaris, J. A., Coutley, R. L., Schiff, L. B., and Platzer, M. F., "Numerical Investigation of High Incidence Flow over a Double-Delta Wing," *Journal of Aircraft*, Vol. 32, No. 3, 1995, pp. 457–463.

[4]Verhaagen, N. G., Jenkins, L. N., Kern, S. B., and Washburn, A. E., "A Study of the Vortex Flow over a 76/40-deg Double-Delta Wing," AIAA Paper 95-0650, Jan. 1995; also Inst. for Computer Applications in Science and Engineering, CR 95-5, NASA LaRC, Hampton, VA, Feb. 1995.

[5]Hebbar, S. K., Platzer, M. F., and Fritzelas, A. E., "Reynolds Number Effects on the Vortical-Flow Structure Generated by a Double-Delta Wing," *Experiments in Fluids*, Vol. 28, 2000, pp. 206–216.

[6]Rogers, D. J., and Verhaagen, N. G., "An Experimental Investigation of the Vortex Flow over a 76/40-deg Double-Delta Wing," Delft Univ. of Technology, Rept. LSW 93-03, Delft, The Netherlands, June 1993.

[7]Visser, K. D., and Washburn, A. E., "Transition Behavior on Flat Plate Delta Wings," AIAA Paper 94-1850, June 1994.

[8]Sellers, W. L., III, and Kjelgaard, S. O., "The Basic Aerodynamics Research Tunnel," AIAA Paper 88-1997, May 1988.

[9]Hummel, D., "On the Vortex Formation over a Slender Wing at Large Angles of Incidence," AGARD CP-247, *High Angle of Attack Aerodynamics*, 1979; also Paper 15, 17 pages (15-1–15-17), *Proceedings of the AGARD Fluid Panel Symposium*, AGARD ISBN 92-835-0230-2, Sandefjord, Norway, Oct. 1978.

[10]Verhaagen, N. G., "Tunnel Wall Effect on the Flow Around a 76/40-deg Double-Delta Wing," AIAA Paper 98-0312, Jan. 1998.

[11]Cunningham, A. M., and Den Boer, R. G., "Low-Speed Unsteady Aerodynamics of a Pitching Strake Wing at High Incidence—Part II: Harmonic Analysis," *Journal of Aircraft*, Vol. 27, No. 1, 1990, pp. 31–41.